ELSEVIER

Journal of Fluids and Structures 25 (2009) 406–419

JOURNAL OF FLUIDS AND STRUCTURES

www.elsevier.com/locate/jfs

Bottom slamming for a Very Large Floating Structure: Uncoupled global and slamming analyses

M. Greco[a,b,*], G. Colicchio[a,b], O.M. Faltinsen[b,c]

[a]*INSEAN, The Italian Ship Model Basin, via di Vallerano 139, 00128 Roma, Italy*
[b]*Centre for Ships and Ocean Structures (CeSOS), NTNU, Trondheim, Norway*
[c]*Department of Marine Technology and CeSOS, NTNU, Trondheim, Norway*

Received 19 September 2007; accepted 19 September 2008
Available online 30 November 2008

Abstract

The bottom slamming of a Very Large Floating Structure (VLFS) has been studied with theoretical and numerical tools. The strategies adopted are: (i) a linear analysis for modeling the global motions of the platform, followed by (ii) a fully nonlinear description for the bottom-slamming occurrence. Model (i) is used to examine the global behavior of a VLFS at model and full scales, and model (ii) is applied to investigate the bottom-slamming features in terms of flow evolution and induced pressure and stresses on the platform bottom. Excitation of hydroelastic coupling and occurrence of air cushion are also discussed together with the challenges connected with scaling effects.

Keywords: VLFS; 2-D potential flow; Uncoupled analysis; Linear-global behavior; Fully nonlinear bottom slamming; Air cushion

1. Introduction

The study of the behavior of a Very Large Floating Structure (VLFS) in waves is an important topic for the research community, because of its practical applications to relevant problems such as floating airports. An overview of recent numerical and experimental developments has been given by Ohmatsu (2005). An example of a VLFS pontoon-type arrangement is: length of 5000 m, width of 2000 m, freeboard of 5 m and draft of 1.5 m; the operational water depth may vary from shallow water to open ocean. The horizontal dimension being much larger than the vertical one makes the elastic behavior significant and implies challenges for physical and numerical models (as discussed in Section 3.2). The assessment of pontoon-type airports in the Japanese area motivated model tests and numerical investigations of this kind of structure. The numerical models have been based on linear hydroelastic analysis of the wave-induced motions and loads on the platform. A VLFS survival condition could be characterized by a significant wave height of 3.7 m and significant wave period of 6.1 s (Watanabe, 2002): therefore diffraction generally matters and may lead to the occurrence of local phenomena such as bottom slamming in the wave-side portion of the platform. The slamming leads to stresses that can be dangerous for the structural integrity, depending on the features of the VLFS. Moreover, the vibrations induced by slamming may cause noise, and undermine the comfort of the passengers on a floating airport.

*Corresponding author at: INSEAN, The Italian Ship Model Basin, via di Vallerano 139, 00128 Roma, Italy. Tel.: +39 0650299343; fax: +39 065070619.
E-mail address: m.greco@insean.it (M. Greco).

0889-9746/$ - see front matter © 2008 Elsevier Ltd. All rights reserved.
doi:10.1016/j.jfluidstructs.2008.09.002

They also modify the local slope of the platform and could compromise the effectiveness of the visual indicator of the incident angle for a landing airplane (PAPI). 2-D experiments of bottom slamming have been performed by Yoshimoto et al. (1997). Bottom-slamming induced pressures were examined theoretically by Takagi (1997) through a 2-D flow solution.

The present study characterizes the global behavior of a VLFS and identifies some important features of slamming phenomena. The structure is modeled as a barge, which is relevant to a pontoon-type VLFS. Head-sea conditions are assumed. In these circumstances 3-D effects are limited due to the very large horizontal dimensions of VLFS. So the problem is simplified as 2-D in the longitudinal plane of the platform and studied with theoretical and numerical tools. One must note that the head-sea assumption would not be suitable to investigate runways installed parallel to the coast line. In this case one could still model the flow as 2-D but along the transversal plane of the platform subjected to beam sea conditions. Two kinds of investigation tools are applied: (i) a linear analysis to study the global motions of the platform, based on the modal approach and a linear-beam model for the structure, and (ii) a fully nonlinear hydrodynamic analysis combined with a linear-beam model to investigate the local bottom slamming. Progress of this research activity has been reported for instance in Greco et al. (2003, 2006). The present work aims to document the whole analysis in terms of the major findings and incorporates previous results with undocumented global and local results. The novelties of this research are: the investigation of the VLFS structural-rigidity influence; the full-scale analysis; the analysis of the bottom loads induced by slamming; the comparative study of hydroelastic effects during slamming events involving an air-cavity entrapment when either a high-speed jet is formed or not.

The basic assumptions of the two complementary solution methods are briefly described in Section 2, the global linear analysis and results are discussed in Section 3 and the local fully nonlinear study is presented in Section 4. Finally a brief summary of conclusions is given.

2. General assumptions

This study deals with high Weber (larger than 10^4) and Reynolds (larger than 10^6) numbers, as in practical full-scale cases, and unseparated flow conditions. Under these assumptions surface-tension effects are unimportant; the vorticity remains concentrated in thin boundary layers; the viscous effects, connected with such thin layers, can be neglected.

In this framework, a potential-flow model is used to describe quantitatively the flow field, the wave field around the VLFS and the induced pressure distribution. The investigation takes into account head regular incoming waves in finite water depth over a flat horizontal sea floor. The problem is simplified analyzing only the center plane of the platform in the wave direction, so the VLFS is seen as a 2-D barge that can deform according to the linear Euler-beam model. No structural damping is modeled and current effects are not accounted for. The sketch of the problem and the main geometrical parameters are given in Fig. 1.

In principle, the global behavior of the platform and the occurrence and features of local phenomena, such as bottom slamming, affect each other and must be investigated within a coupled analysis. In the following, the coupling is neglected and the global and local analyses are studied separately to gain fundamental insights of the involved physical phenomena. This assumption becomes questionable when the platform motions are not small. In such circumstances the coupling could be handled for instance using the solution algorithm in Fig. 2 described by Greco et al. (2008).

3. Linear-global analysis: method and studies

Here the hydroelastic strategy developed to analyze the global behavior of a VLFS is presented and some results discussed.

3.1. Solution method

Neglecting the occurrence of local nonlinear phenomena the global motions of a 2-D floating platform can be studied through the equations

$$[M_{ij} + a_{ij}(\omega = \infty)]\ddot{\xi}_j(t) + [c_{ij} + k_{ij}]\xi_j(t) + \int_0^t h_{ij}(\tau)\,\dot{\xi}_j(t-\tau)\,\mathrm{d}\tau = F_{\mathrm{exci},i}(t) \tag{1}$$

for each mode amplitude ξ_j, being $j = 1 =$ surge, $2 =$ heave, $3 =$ pitch and $4 \ldots Nb + 3 =$ beam modes. In Eq. (1), M_{ij}, $a_{ij}(\omega = \infty)$, c_{ij}, k_{ij} and h_{ij} are, respectively, the generalized [e.g. see Faltinsen (1997)] mass, infinite-frequency added

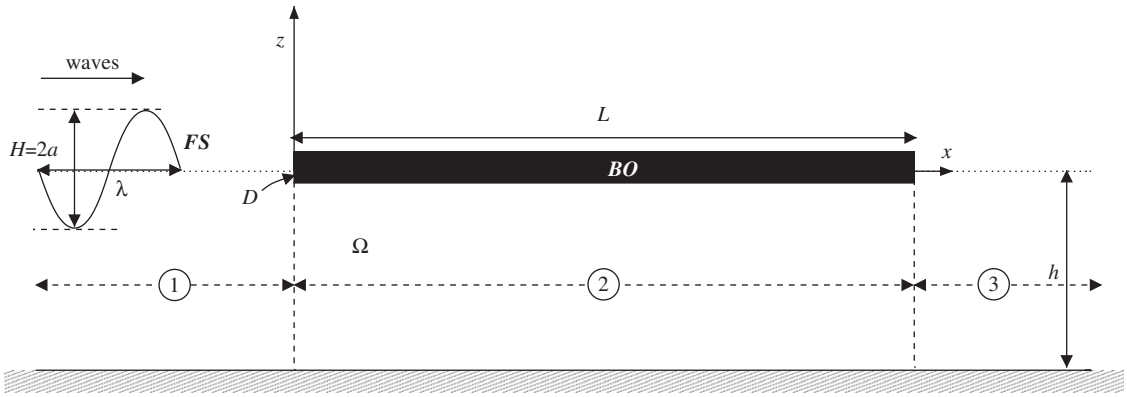

Fig. 1. Sketch of the problem and definition of the main parameters. Subdomains 1, 2 and 3 are used to solve the radiation and diffraction problems in the linear-global analysis of Section 3.

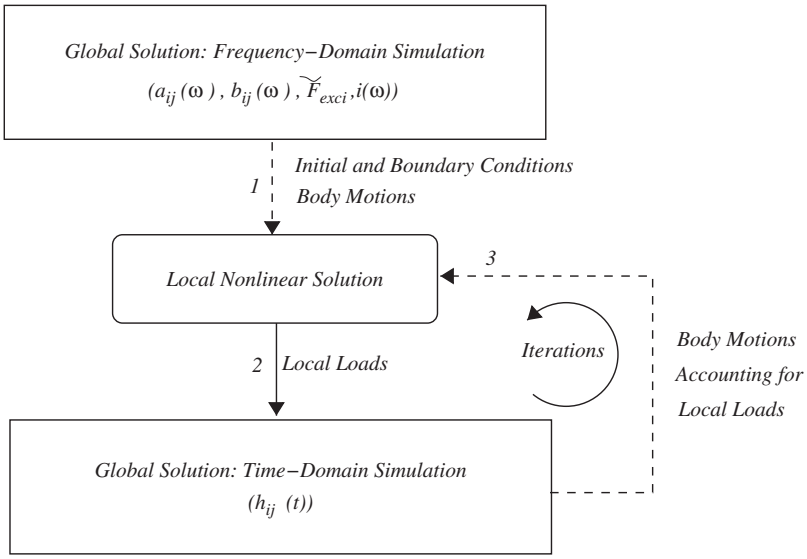

Fig. 2. Strategy for the iterative coupling between local and global solutions.

mass, hydrostatic restoring, structural stiffness and retardation-function matrices and $F_{\mathrm{exci},i}$ represent the generalized excitation loads. The upper dots on ξ_j stand for time derivatives.

The linear problem (1) can be solved efficiently in the frequency domain, assuming regular incoming waves with frequency ω and steady-state conditions, i.e. $\xi_j(t) = \Re[\tilde{\xi}_j(\omega)\,\mathrm{e}^{-\mathrm{i}\omega t}]$. The introduction of these assumptions in Eq. (1) leads to

$$\{-\omega^2[M_{ij} + a_{ij}(\omega)] - \mathrm{i}\omega\, b_{ij}(\omega) + c_{ij} + k_{ij}\}\tilde{\xi}_j(\omega) = \tilde{F}_{\mathrm{exci},i}, \tag{2}$$

where $F_{\mathrm{exci},i}(t) = \Re[\tilde{F}_{\mathrm{exci},i}(\omega)\,\mathrm{e}^{-\mathrm{i}\omega t}]$. To solve the problem all the terms of the equations of motion must be evaluated. The generalized mass, structural-stiffness and hydrostatic restoring coefficients are known using structural and dimensional details of the platform while the hydrodynamic terms are found solving the radiation and diffraction problems for the velocity potentials

$$\varphi_j(x,z,t) = \Re[\phi_j(x,z)\,\dot{\tilde{\xi}}_j(t)] = \Re[\phi_j(x,z)\,\tilde{\xi}_j\,\mathrm{e}^{-\mathrm{i}\omega t}(-\mathrm{i}\omega)], \quad j = 0,\ldots,N_b+3, \tag{3}$$

where $j = 0$ and $j > 0$ represent, respectively, the diffraction and radiation potentials. In expressions (3) the variable separation principle has been applied. The related problems are solved following the strategy suggested in Fig. 1: the fluid domain is split into the sub-regions $d = 1$, 2 and 3, respectively, upstream, under and downstream of the platform,

and in each of them a local velocity potential is defined. The diffraction and radiation problems are analyzed simultaneously using the solution algorithm developed by Johansson (1989) for a rigid 2-D barge and extended here with the inclusion of a linear elastic beam model. As for the rigid case, the radiation problem associated to each beam mode ($j>3$) requires the estimate of a velocity potential satisfying homogeneous boundary conditions everywhere but on the body where the normal velocity is consistent with the velocity of deformation of the jth mode. Once the velocity potentials are known for all the problems, the added-mass coefficients, the damping coefficients and the excitation forces can be calculated.

The effectiveness of the method has been successfully verified in terms of frequency-dependent added-mass and damping coefficients and motion amplitudes, and validated in terms of displacement and pressure amplitude distributions along the platform. Most of the results have been reported in Greco et al. (2006).

3.2. Physical investigations

A parameter study of the VLFS global behavior has been carried out by examining the four cases given in Table 1. The implications for bottom-slamming occurrence are also pointed out.

The first two studies concern 3-D model tests, respectively, by Yago and Endo (1996) and Ohta and Ohmatsu (1998). The former studied the interactions of the Mega-float phase I model with regular incoming waves with wavelength-to-platform width ratio $\lambda/W \in [1, 5]$; the latter tested a runway model using $\lambda/W \in [0.25, 0.9]$. The third study corresponds to the 2-D experiment by Yoshimoto et al. (1997) on two VLFS models, A and B, designed with different stiffnesses. Yoshimoto et al. take the draft, D, as main reference parameter while the length of their model does not respect the typical L/D ratio and is much smaller than it should be. So, for this experiment the incoming wavelength must be referred to the draft, in particular $\lambda/D \simeq 60$ would correspond to survival conditions. The last study deals with a full-scale VLFS concept. The structural and geometrical properties have been taken from Yoshimoto et al. (1997) and the platform is modeled as a cantilever beam with restrained rigid body motions, as it would be the case for a floating structure connected rigidly to the sea floor on the lee side.

The following investigation is based on results in Greco et al. (2006) coupled with new results related to the influence of the VLFS structural features and to the full-scale analysis.

3.2.1. Influence of 3-D effects and structural damping

Generally, 3-D effects and structural damping have to be considered in reality. The platform displacements measured by Yago and Endo (1996) show a good agreement with 3-D BEM results (see Fig. 3, where L is the length of the platform, w is the displacement and a is the wave amplitude). The 3-D results were obtained assuming zero structural damping [private communication from Taghipour; the solver is described in Taghipour et al. (2006)]. This indicates a negligible role of structural damping in these model tests. The comparison with the present 2-D solution highlights that the 3-D effects are limited in the upwave region, cause a lower response amplitude further downstream along the platform and they reduce the importance of higher modes. Globally the poorest 2-D results were obtained for $\lambda/W = 2$ (i.e. $\lambda/L = 0.4$) and the discrepancies reduce for larger or smaller wavelengths. The same improvement in 2-D results for smaller λ/W was found for study No. 2 which examined incoming waves with $\lambda/W < 1$. In this case no 3-D numerical results were available so no further comments can be made.

For a typical full-scale VLFS one should expect $\lambda/W \ll 1$, and in this wavelength range the analysis suggests that a 2-D model could be a reasonable tool for investigating in the case of head-sea conditions, especially on the upwave end where slamming phenomena can occur. The effect of high elastic modes should therefore be considered only in the upstream portion of the VLFS. Fig. 4 shows that, for incoming waves with $\lambda = 0.1L$, the 24th mode (corresponding to

Table 1
Experimental studies examined. Study 1: Yago and Endo (1996). Study 2: Ohta and Ohmatsu (1998). Study 3: Yoshimoto et al. (1997). Study 4: full-scale VLFS concept

Study	Length (L) (m)	Draft (D) (m)	Bending stiffness (EI) (N m^2)	Water depth (h) (m)	Width (W) (m)
1	300	0.5	46.892×10^{10}	58.5	60
2	1200	1.0	1.0704×10^{13}	20	240
3	5.3	0.027	A: 19 676, B: 288 551	2	–
4	5000	1.5	4.05×10^{9}	20	–

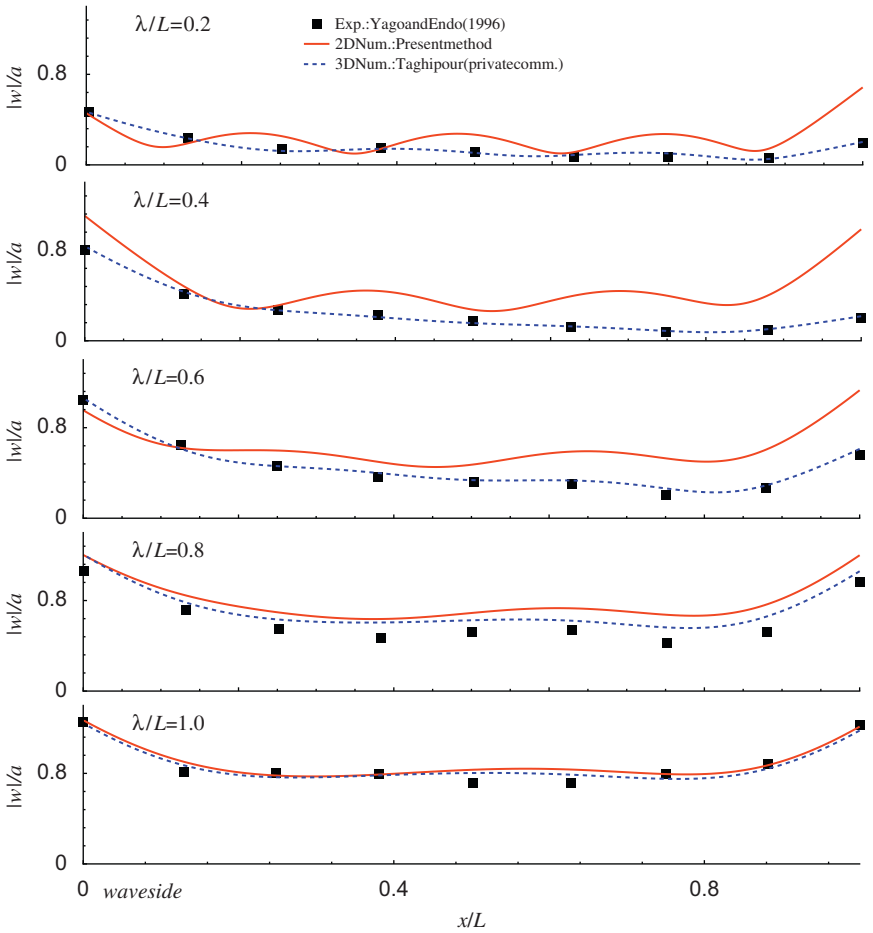

Fig. 3. Global investigations: study 1 of Table 1. Beam displacement for different λ/L ($L/W = 5$).

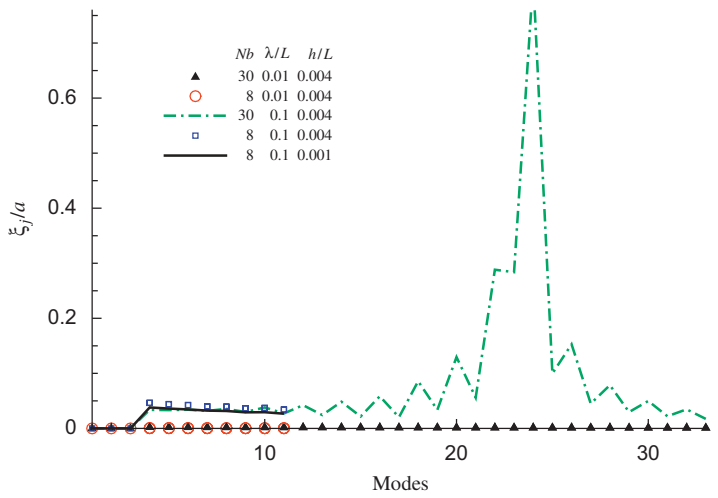

Fig. 4. Global full-scale investigation. Mode amplitudes. *Nb* is the number of beam modes used.

the 21 beam mode) makes the largest contribution. The curve of the modal amplitude is affected by clear oscillations for modes higher than the 10th. These are connected with numerical errors that arise when studying very long structures (i.e. $L \gg D$ and $L \gg h$) because the corresponding radiation and scattering problems involve the estimates of hyperbolic and trigonometric functions of large arguments. On the other hand, the high modes characterize the bottom structural behavior in the upwave region and should be modeled there.

To avoid such errors and recover a better description of bottom-slamming events, here the following 2-D approach is proposed. A low number of modes is used to describe the global structure, coupled with a local upstream analysis that models the upwave portion of the platform with a high number of modes. In fact, for the examined case, Fig. 4 shows that the use of $N_b = 8$ modes avoids the oscillations and provides modal amplitudes consistent with those estimated with 30 modes. The amplitude for the first eight modes is limited and smaller than 5% of the incoming wave amplitude a. From the physical point of view, $\lambda = 0.1L$ means a wavelength of 500 m, which is quite a long wave. Survival conditions would be characterized by much shorter waves with $\lambda \simeq 0.012L$ (corresponding to the peak period). For such wavelength, $\lambda = 0.01L$, the results in Fig. 4 show very limited elastic motions of the structure, with modal amplitudes smaller than $0.0005a$. This is consistent with what has already been discussed, and suggests that for such wave conditions the bottom slamming could be investigated neglecting the global motions of the platform as a first step.

3.2.2. *Influence of structural rigidity*

The analysis of the two VLFS models used in study No. 3 furnishes some insights about the influence of structural rigidity on the platform behavior in waves. The values of the Young modulus were not available from the model tests. The lack was overcome assuming in the simulations Aluminum for model A and steel for model B. The amplification of a factor of 15 in the rigidity is responsible for a reduction by a factor of three in the motions in the upwave portion of the platform (see for example Fig. 5 for $\lambda/D = 65$). This is relevant in terms of bottom-slamming occurrence.

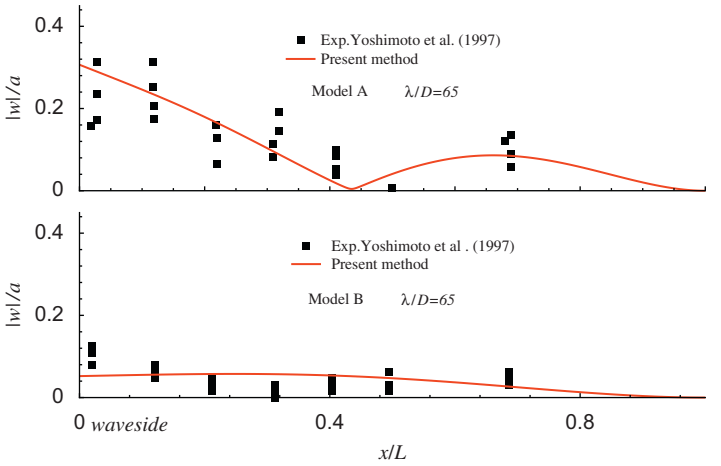

Fig. 5. Global investigations: study 3 of Table 1. Beam displacement for two values of the structural rigidity.

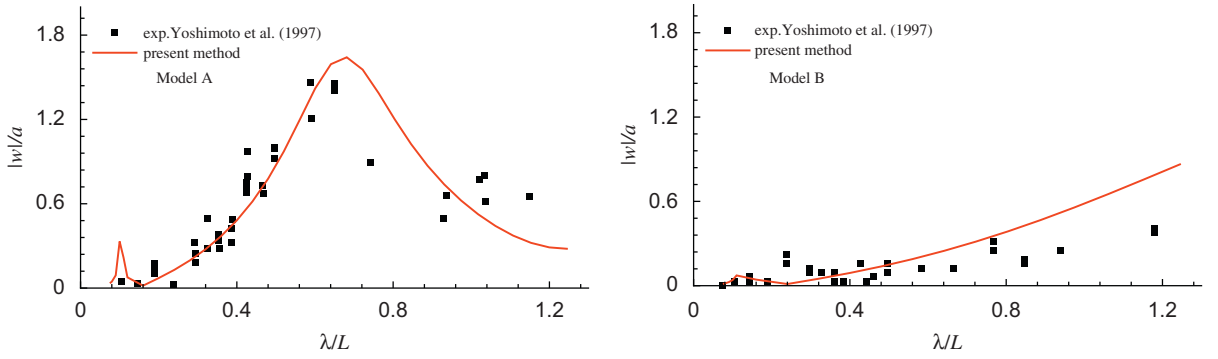

Fig. 6. Displacement amplitude at $x = 0.025L$ from the upwave end for model A (left) and B (right).

The structural properties affect the resonance features. This is shown in Fig. 6 in terms of the displacement amplitude at $x = 0.025L$ from the upwave end as a function of λ/L for models A and B. It is seen in the figure that an increase in rigidity leads to a reduction in the amplitude of motion. This suggests that adequate stiffening of the platform would lead to very limited global motions in the case of incoming waves with $\lambda \ll L$. It implies that slamming events may occur on an almost fixed platform but the slamming occurrence could induce local deformations and affect the global behavior.

Other sources of influence are analyzed only briefly in the following.

3.2.3. Dominant modes

Study No. 1 was used to investigate numerically the importance of the different modes on the global VLFS behavior [see Greco et al. (2006)]. Varying λ between $0.2L$ and L, the elastic modes were found always dominant with respect to the rigid motions. However, as λ/L reduces the maximum amplitude moves toward higher beam modes and its value decreases. A higher number of elastic modes matters and they could couple with rigid modes, whenever allowed. The actual value of the amplitude of the high modes could be reduced also by other factors, for instance by 3-D effects as discussed above.

3.2.4. Influence of draft and water depth

The analysis confirmed a negligible direct effect of the draft, D, on the global behavior of a VLFS. However, D can matter both directly and indirectly. For instance, it is strongly connected with the rigidity of the structure which affects the platform motions, as discussed above. Furthermore, D influences the occurrence and features of bottom slamming.

To investigate the effect of water depth h, this was varied from 20 to 5 m in study No. 4. The results did not show any substantial difference in terms of modal amplitudes (see Fig. 4 for $\lambda/L = 0.1$). This suggests that the direct effect of the water depth is limited. However, a smaller h modifies the incoming waves and may result in a different local interaction with the platform, in particular in terms of occurrence and features of bottom-slamming events. This could lead to an indirect effect on the global motions of the platform.

4. Local fully nonlinear analysis: method and studies

In the following, the occurrence and features of bottom slamming and subsequent local effects on the structure are examined by means of a fully nonlinear analysis. Based on the results from the linear studies in Section 3, the rigid motions are restrained and the elastic deflections are modeled only in the upstream portion of the platform. As a result the platform length L does not affect the details of the flow in the upwave region and can be reduced to limit the CPU-time requirements as long as it is chosen large enough with respect to the platform draft. Here $L/D = 120$ is used. The water depth is chosen to be sufficiently large (with respect to the incoming wavelengths studied) that it does not affect the solution. As a consequence the parameters of the problem are: D, λ (or alternatively the incoming wave period T) and H.

4.1. Solution method

As shown in Fig. 1, the liquid domain $\Omega(t)$ is bounded by the free surface FS, the wetted surface of the 2-D VLFS, BO, and an outer surface $\partial\Omega_{\text{outer}}$. The latter is formed by a flap wave-maker, WM, placed at $240D$ upstream of the platform wave-side, the horizontal bottom and a downstream control surface. Incoming waves generated by WM are damped out downstream of the VLFS using a numerical wave beach. This provides a limit on the fluid domain and avoids unphysical wave reflection.

The flow evolution is analyzed in terms of the velocity potential $\varphi(\vec{P}, t)$ by fully retaining nonlinearities associated with the motion of the free surface. Along the free and solid boundaries the kinematic condition limits the fluid particles to have the same normal velocity as the corresponding geometrical points of the surface. The dynamic free-surface condition requires that the pressure $p(t)$ at the free surface is balanced by the instantaneous ambient pressure $p_a(t)$. Usually p_a coincides with the atmospheric pressure but becomes a time-varying pressure when for instance air entrapment occurs. In such circumstances, it is assumed that there is no leakage and the air is modeled as an ideal gas in adiabatic conditions with pressure $p_a(t)$ and volume $S(t)$ linked by

$$p_a(t) = p_a(t_0)\left[\frac{S(t_0)}{S(t)}\right]^{\gamma}. \tag{4}$$

Here $p_a(t_0)$ and $S(t_0)$ are, respectively, the pressure and the volume of the air cavity at the time instant t_0 when the cavity is formed and $\gamma = 1.4$. The pressure along BO is computed by the Bernoulli equation and the force follows by direct pressure integration.

The problem is solved numerically using the Mixed Eulerian–Lagrangian strategy (Ogilvie, 1967) and adopting a Lagrangian description to follow the FS evolution. At any time instant the boundary value problem (b.v.p.) for the velocity potential is solved through the Boundary Element Method [BEM, Greco (2001)] knowing φ along FS and its normal derivative along the solid boundaries. The evaluation of the pressure along the body-wetted surface BO requires the rate-of-change $\partial\varphi/\partial t$ of the velocity potential which is found by solving a problem formally equivalent to the b.v.p. for φ, in the case of a rigid platform. A standard fourth-order Runge–Kutta scheme is adopted to step forward in time the evolution equations of the problem. A detailed description of the method can be found in Greco (2001).

In some circumstances, the water–body interactions may induce elastic deflections of the structure on spatial and time scales such that the deflections in turn affect the fluid motion. When this occurs the fluid-dynamic and structural problems should be coupled. To assess the importance of hydroelasticity in connection with bottom slamming, the leading portion of the platform bottom is modeled as a linear Euler beam deforming according to the equation

$$m\frac{\partial^2 w}{\partial t^2} + EI\frac{\partial^4 w}{\partial \zeta^4} = -\rho\left(\frac{1}{2}|\nabla\varphi|^2 + \frac{\partial\varphi}{\partial t} - \vec{g}\cdot\vec{P}\right). \tag{5}$$

Here w is the beam deformation at the location ζ and the right-hand-side gives the pressure in terms of the Bernoulli equation. ρ is the water density, $\vec{g}$ is the vector of acceleration due to gravity, the vector $\vec{P}$ defines a point on the deformed beam, m is the structural mass per unit length and EI is the beam bending stiffness. Assuming that at a given instant of time the beam geometry w, the deflection velocity $\partial w/\partial t$ and the other suitable boundary data along free and rigid surfaces are known, then the b.v.p. for the velocity potential φ can be solved. The hydrodynamic pressure forcing the beam depends on $\partial\varphi/\partial t$ whose b.v.p. involves a non-homogeneous Robin condition along the elastic portion of the platform [see Greco et al. (2004)]. Within the solution strategy, the transverse deformation $w(\zeta, t)$ is expressed in terms of N beam dry modes and the solution is found in terms of the unknown time-dependent coefficients.

When bottom slamming occurs the solution algorithm shown in Fig. 7 is adopted. Typically the water hits the upwave bottom end of the VLFS bottom. The angle between the free surface and the bottom, say β, is small and very rapid changes of the wetted area are expected at the end. To avoid numerical instabilities and to handle accurately the impact, a local high-speed analytical solution for a liquid wedge with half-angle β hitting a flat bottom is incorporated in the global numerical method. The local strategy follows the work by Wagner (1932) and is documented in Faltinsen et al. (2004). At the impact instant t_{imp}, the local solution is introduced at the water region near the upwave-bottom end where the free-surface forms an angle $\beta \pm \varepsilon$ with the body surface, where $\varepsilon < 1^\circ$. The time duration Δt of the analytical

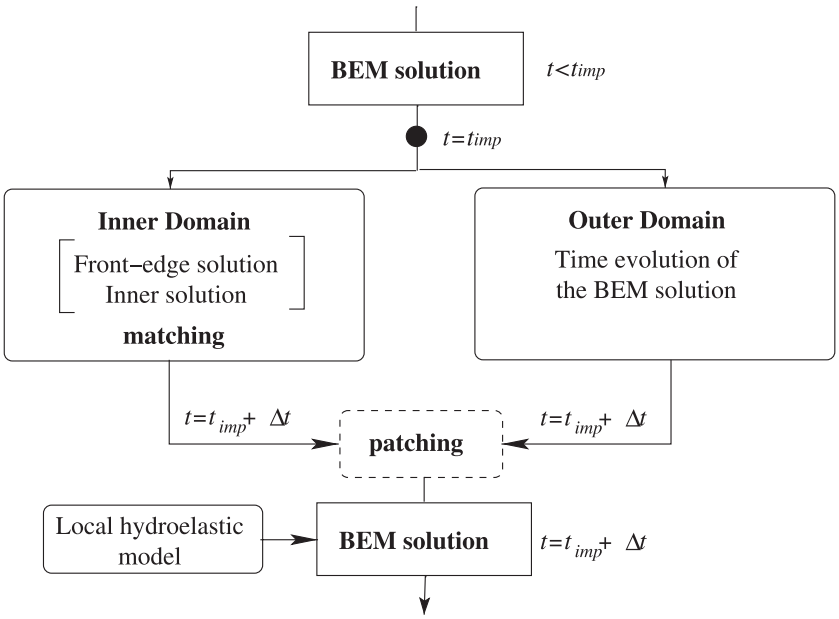

Fig. 7. Fully nonlinear investigation. Solution algorithm for the bottom-slamming analysis.

slamming is determined by deciding the maximum wetted length $2c = 4V_0\Delta t/3\tan(\beta)$. Here V_0 is the entry velocity assumed constant and equal to the water impact velocity. The free-surface elevation at the time $t_{\text{imp}} + \Delta t$ is composed of two parts: in the outer part, the free-surface particles are moved with the BEM velocity at time t_{imp}; in the inner domain, the wave elevation is determined by the local solution while the velocity potential on *FS* is not affected by the impact (i.e. the dynamic free-surface condition for the local problem is $\varphi_{\text{imp}} = 0$) and its value at time $t_{\text{imp}} + \Delta t$ is obtained by integrating the rate of change of φ predicted by the BEM at time t_{imp} using an Euler time-stepping scheme. Once the BEM and the local analytical solution are patched at the time $t_{\text{imp}} + \Delta t$, the further flow evolution can be described again by the BEM only. The latter includes the modeling of air compressibility in entrapped cavities and the hydroelastic coupling (when of interest) with the structure.

4.2. Physical investigations

The bottom slamming has been partially investigated in Greco et al. (2003) for selected combinations of the incoming wave parameters in the ranges $H/D \in [3.2, 6.3]$ and $T(g/D)^{1/2} \in [21.0, 31.1]$. The cases were chosen to have water-entry and exit phases with different severity. Here the main outcomes of the physical analysis are summarized and incorporated with additional investigations related to the bottom pressure and evolution of the structural stresses induced by slamming. The slamming scenarios with air entrainment are examined using the first two impacts caused by incoming waves with $H/D = 4.9$ and $T(g/D)^{1/2} = 21.5$, respectively, referred to as first and second impact in the following.

4.2.1. General features

Within the wavelength range examined, the wave–structure interaction causes diffraction of the incident waves. In the most severe cases, during water run-down the free surface reaches the bottom of the structure and turns rapidly around the upwave-bottom end. To avoid numerical problems, in the simulations the edge is rounded with a radius of $0.2D$. This proved to have a negligible effect on the results [see e.g. Faltinsen et al. (2004)]. For small values of H/λ the local free surface is relatively flat while for higher values it has a large curvature and forms a small angle with the structure. The resulting water-exit phase can be characterized by a relatively steep variation in the pressure distribution along the structure. The maximum extension, say $l_{d,\max}$, of the bottom emergence is a measure of the bottom area affected by slamming and increases with H/D. The $l_{d,\max}$ predicted by the present nonlinear-potential solver agrees well with the measurements by Yoshimoto et al. (1997), as shown by Greco et al. (2003). This indicates a limited influence of vortex shedding connected with cross-flow at the upwave-bottom end. The comparison with the linear solution by Yoshimoto et al. (1997) for $l_{d,\max}$ highlights the importance of nonlinear effects.

A new water rise-up phase counteracts the water-exit and may cause a water impact with the platform bottom. It is associated with the entrapment of an air cavity for all the slamming events examined. In the present model the air is not simulated before the impact. This can represent an error source in the prediction both of the shape and pressure of the entrapped air and of the occurrence of air entrainment, i.e. the air could escape and prevent the formation of an air cavity. Such error sources are directly connected with the single-phase strategy. However, 3-D effects may play a greater role in realistic sea conditions.

For all the analyzed bottom-slamming events the impact angle β was in the range from a few to 12°, so they were handled by the method outlined in Section 4.1. In the figures of the following discussion $t = 0\,\text{s}$ represents the time instant of the impact event studied. Figs. 8 and 9 show the first two bottom impacts for incoming waves with $H/D = 4.9$ and $T(g/D)^{1/2} = 21.5$. The first event is characterized by $\beta = 3.6^\circ$ and $V_0 = 0.428\sqrt{gD}$, and the second by $\beta = 11.5^\circ$ and $V_0 = 0.848\sqrt{gD}$. The area of the cavity entrapped during the first impact is $1.5D^2$ while it is eight times larger in the second impact. Due to the cavity entrapment the Euler number $Eu = p_a/\rho V^2$, governing the compressibility of the inner air, becomes an additional parameter of the problem. Taking the impact velocity V_0 as reference velocity V, for the first and second impacts $Eu \simeq 38$ and 10, respectively. The limited value of Eu combined with a larger area induces a quick formation of a jet flow in the second impact, not observed during the first event. The different features between the two impacts are responsible for loads of different magnitude on the platform (see top parts of Figs. 8 and 9).

Both events are characterized by a sudden peaked increase of the pressure due to the impact. During the first impact, the initial free-surface configuration shown refers to the time instant when the local analytical solution is patched with the BEM solution, i.e. $t = t_{\text{imp}} + \Delta t$; so the related pressure curve coincides with the analytical pressure solution $p_{\text{theo}} = \rho V_0\sqrt{x}(\mathrm{d}c/\mathrm{d}t)/\sqrt{2c - x}$ of the Wagner-type problem mentioned in Section 4.1. The value of the pressure peak, obtained by evaluating the composite solution between the inner and outer (given by p_{theo}) solutions, could play a role in influencing the local structural design. However, due to the small time scales involved, in practical applications the pressure impulse is of more concern than the pressure maximum value. After the impact the bottom pressure reduces

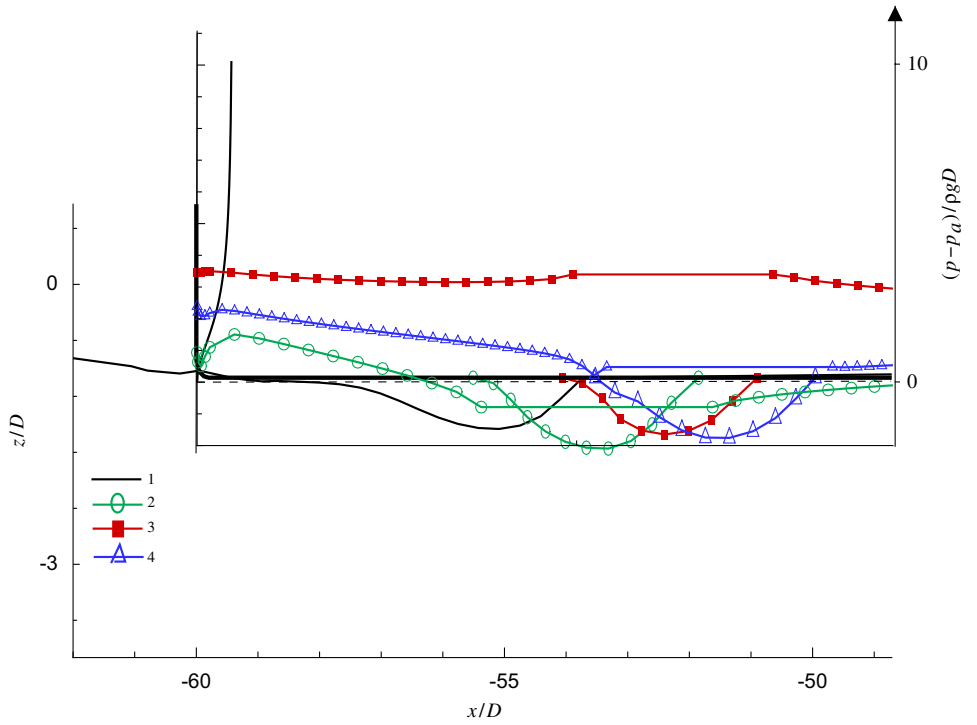

Fig. 8. Fully nonlinear investigation: first bottom impact. Top: pressure evolution. Bottom: free-surface evolution. Rigid-bottom solution. The configurations are enumerated as time increase and correspond to $t = 0.0028, 0.168, 0.245$ and $0.302T$.

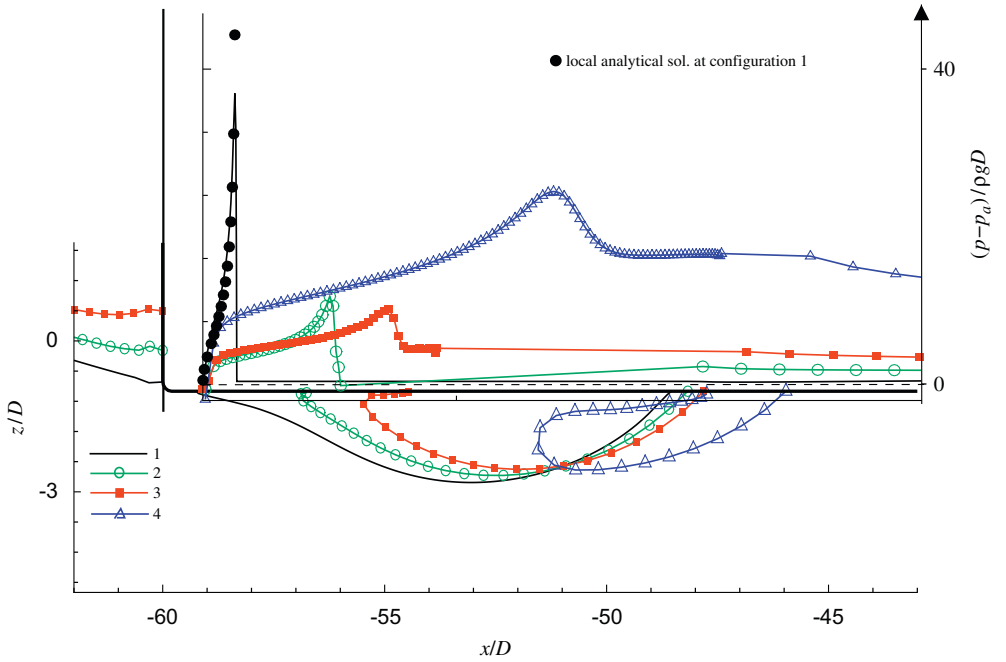

Fig. 9. Fully nonlinear investigation: second bottom impact. Top: pressure evolution. Bottom: free-surface evolution. Rigid-bottom solution. The configurations are enumerated as time increase and correspond to $t = 0.005, 0.024, 0.043$ and $0.099T$. The symbols are the analytical pressure from Wagner-type method used to handle the slamming.

rapidly and its evolution is governed by the cavity motion. The pressure oscillates in time, following the volume pulsation of the entrapped cavity with a period much smaller than the wave period (see later Fig. 14).

The first configuration of the second slamming event refers to the full BEM solution, i.e. $t > t_{\text{imp}} + \Delta t$. The corresponding pressure distribution in the impact zone compares well with the local analytical Wagner-type pressure. As time advances the pressure preserves the peaked behavior due to the inward jet. The pressure peak occurs near the jet root and exceeds the pressure inside the cavity. The formation of a jet is numerically challenging in terms of convergence. In the present studies, refining the discretization shows that the global solution remains practical identical but locally the predicted jet speed tends to reduce, lowering the pressure. This represents an error source in the hydroelastic problem, because the pressure is the link between the fluid and structural problems.

4.2.2. *Hydroelastic effects*

Here, the fluid–structure coupling is described during the two bottom impacts. The structural features of the VLFS bottom are modeled in the wave-side region by introducing a beam equivalent to the stiffened bottom plating with longitudinal stiffeners between two transverse stiffeners. Fig. 10 shows their arrangement and the section of the equivalent beam with the position of the neutral axis. Only the equivalent beam at the upwave end is considered, while the rest of the VLFS bottom is assumed rigid. The beam has a length $L_b = 5\,\text{m}$ and is clamped at the ends. The case study considers a structural mass per unit length and breadth $240.7\,\text{kg/m}^2$, beam bending stiffness $EI \simeq 27.5\,\text{MN m}^2/\text{m}$ and no structural damping. Three solution strategies are considered: (a) the pressure is evaluated assuming a rigid platform bottom; (b) an infinite-frequency added-mass correction is introduced to include the effect of water [details can be found in Faltinsen et al. (2004)]; (c) a full-hydroelastic analysis is performed, as described in Section 4.1.

Figs. 11 and 12 show the time evolutions of the pressure inside the cavity and of the maximum stresses on the beam for the two events. At any time instant the maximum tension and compression stresses are evaluated at the beam section with the largest magnitude of the bending moment: they correspond, respectively, to the maximum positive and negative stress relative to the sectional neutral axis. The evolution of the cavity pressure for the two impacts is not affected by a full-hydroelastic analysis. This is because in both cases the cavity disappears relatively quickly from the elastic portion of the bottom and the beam is fully wetted after $\simeq 0.21$ and $\simeq 0.2\,\text{s}$, respectively. The first impact shows two time scales in the stress evolution. On a large time scale, the stresses follow the cavity-pressure oscillations in a quasi-steady manner. The oscillation period estimated for the cavity is consistent with the value $T_1 \simeq 0.72\,\text{s}$ predicted for the highest natural period by a simplified analysis [see Faltinsen et al. (2004)]. The high-frequency oscillations in the stress curves are related to first-mode vibrations. The wet natural period predicted by the approximate hydroelastic study ($\simeq 0.073\,\text{s}$) is slightly larger than the value predicted by the full-hydroelastic analysis ($\simeq 0.053\,\text{s}$). Both are clearly higher than the dry natural period ($\simeq 0.018\,\text{s}$). The comparison of solutions (b) and (c) suggests a negligible hydroelastic effect. In fact, the stress amplitudes are not much modified by the hydroelastic coupling. This is due to the wetting time of the beam ($\sim$0.24 s) being large relative to the highest wet natural period, and to the absence of sudden changes in the excitation on the time scale of the wet natural period. The maximum absolute value reached by the stresses ($\sim$200 MPa) is comparable with the allowable-stress limit for high-strength steel (about the 70% of the yield stress $\sim 320-360\,\text{MPa}$).

The second bottom-slamming event shows different features. Within the examined time interval the cavity pressure increases monotonically (see left plot of Fig. 12), because of the larger highest natural period of the cavity ($T_1 = 2.28\,\text{s}$). As a result the cavity evolution is 'driven' by the inward jet. Initially the stresses obtained with the methods a, b and c

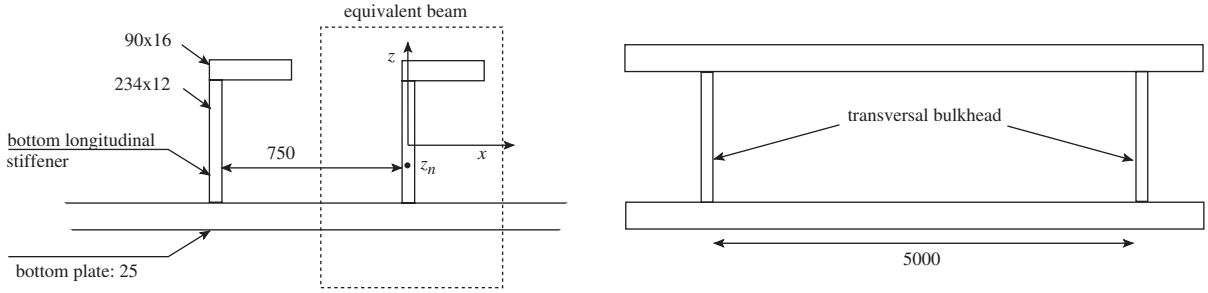

Fig. 10. Qualitative sketch: stiffeners arrangement for the bottom plate of a VLF platform and section of the equivalent beam. Left: transversal view. Right: longitudinal view. The dimensions are in millimeters. The vertical position of the beam-section neutral axis is $z_n \simeq -0.0977\,\text{m}$ in the reference frame with the vertical origin at the middle of the beam section.

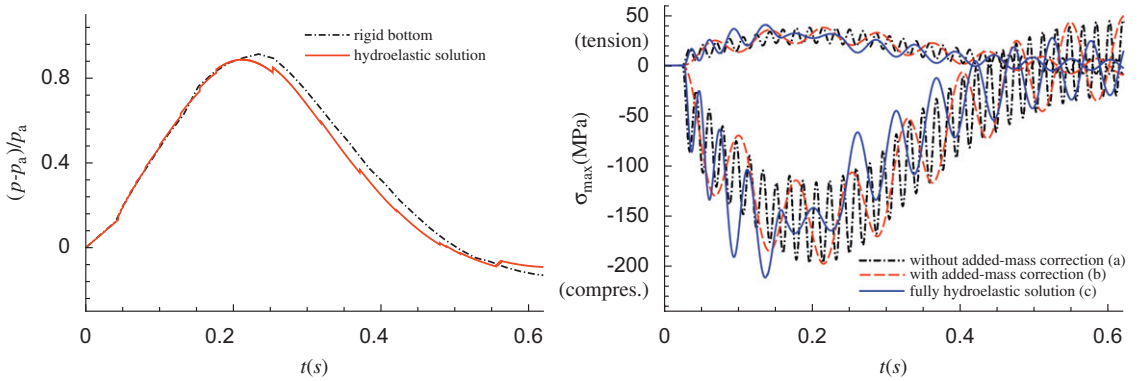

Fig. 11. Fully nonlinear investigation: first bottom impact. Left: relative pressure variation inside the cavity. Right: maximum tension and compression stresses on the beam.

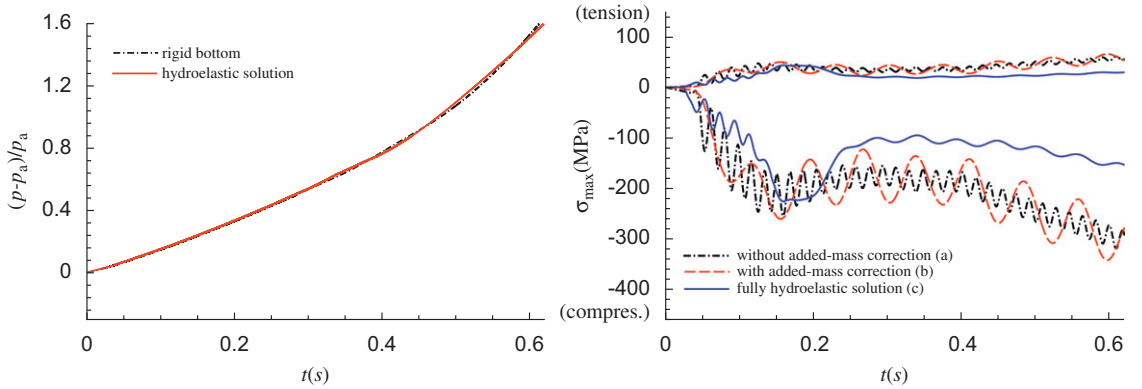

Fig. 12. Fully nonlinear investigation: second bottom impact. Left: relative pressure variation inside the cavity. Right: maximum tension and compression stresses on the beam.

show a similar behavior even though with different high-frequency behavior. As time goes on, the stresses of the full-hydroelastic approach tend to oscillate around values smaller than those predicted by the simplified approaches. This suggests that hydroelasticity matters when large jet formation occurs. For the case examined, there are no visible effects on the free-surface evolution while the pressure on the platform bottom is clearly affected by the structural deflections (see Fig. 13). The stress level for this event remains still high and close to the allowable stress for the structural integrity.

4.2.3. *Scaling effects*

When cavity entrapment occurs the Euler number should be considered to achieve the correct scaling. Experimentally this is hard to achieve and only Froude scaling is satisfied. The limits of the experimental analysis have been investigated numerically by studying platform drafts in the range [0.0135 m, 1.5 m]. As expected, the cavity pressure does not scale with Froude number and its full-scale values can be substantially overestimated, in the considered case, by Froude scaling. For example, for the first bottom impact caused by incoming waves with $H/D = 4.9$ and $T(g/D)^{1/2} = 21.5$, the maximum pressure predicted for a VLFS with draft $D = 1.5$ m is nine times smaller than the value obtained by simply Froude scaling to $D = 1.5$ m the estimate found for $D = 0.027$ m. Froude scaling leads to a model scale Eu larger than the corresponding full-scale value and this may be responsible for physical phenomena which would not occur in reality. For instance, at model scale the local pressure is higher than at full scale relative to the dynamic pressure associated with slamming, so bottom-slamming events could occur without air entrainment while at full scale air would be entrapped [as seen in the example given by Greco et al. (2003)]. This analysis does not account for the effect of the platform motions.

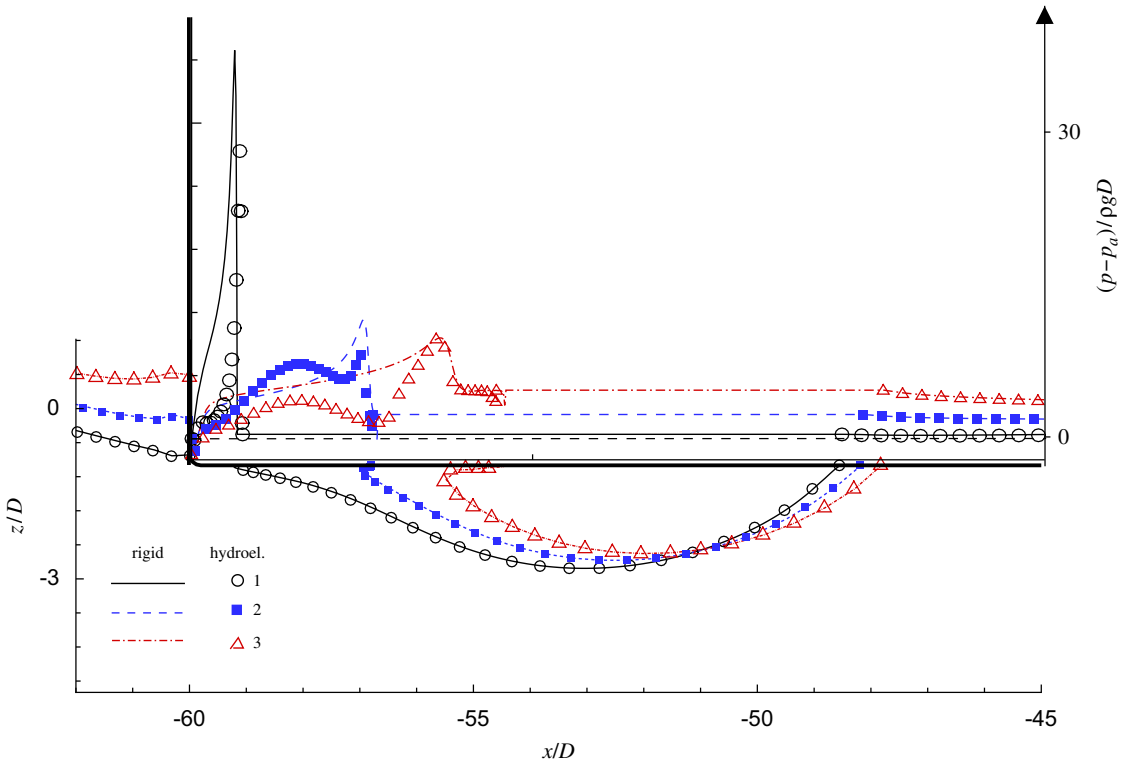

Fig. 13. Fully nonlinear investigation: second bottom impact. Pressure (top) and free-surface (bottom) evolutions during jet development. Rigid-bottom and hydroelastic solutions. The configurations are enumerated as time increase and correspond to $t = 0.005, 0.024$ and $0.043T$.

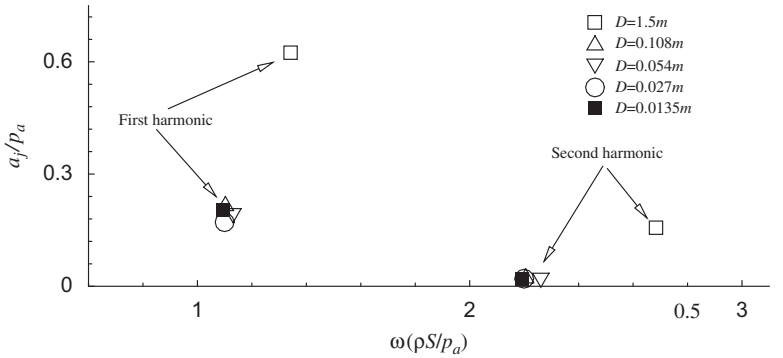

Fig. 14. Scale effects connected with air entrapment: the first two Fourier components of the differential cavity pressure $p - p_a$. S is the volume of the entrapped cavity and ρ is the water density. Incoming waves with $H/D = 4.9$ and $T(g/D)^{1/2} = 21.5$.

The Fourier analysis of the cavity pressure time series for the different cases shows that for small D, the frequencies of the first and second components are roughly consistent with the scaling law predicted by Bagnold (1939) for an oscillating air bubble under a linear assumption (linear scaling: $\omega\sqrt{S}/V_0 \sim \sqrt{\gamma Eu}$, with ω the pulsation frequency of the bubble). The relative pressures of the cavities do not satisfy the corresponding law (linear scaling: $p_{\max}/\rho V^2 \sim \sqrt{\gamma Eu}$, with $p_{\max}$ being the amplitude of pressure oscillations), and they scale roughly with the ambient pressure (see Fig. 14). For $D = 1.5$ m, none of the previous scaling laws are satisfied. From the results it is not obvious how to transfer model-scale results into full-scale information. This requires a deeper investigation, left to a future activity.

5. Conclusions

Bottom-slamming phenomena were investigated in connection with Very Large Floating Structures. Head-sea conditions were assumed, and the problem was solved numerically using 2-D potential-flow theory. The coupling between (1) global behavior of the platform and (2) local phenomena was neglected and (1) and (2) were studied as separated problems. This becomes questionable when the VLFS motions are not small. In such circumstances (1) and (2) must be investigated as coupled problems, as discussed by Greco et al. (2008). A linear-global solver was adopted to investigate the global behavior of the platform and to guide the choices within the analysis of slamming events performed through a fully nonlinear strategy. The main features of the slamming events have been identified and studied in terms of flow evolution and induced pressures on the platform bottom. Hydroelastic effects were examined and their importance has been highlighted in the case of large jets after the slamming. The stress levels induced by slamming appear high and suggest a concern for the local integrity of the structure. The analysis of air cushion phenomena highlighted the challenges in transferring model-scale results to full scale.

Acknowledgments

The present research activity is partially supported by the Centre for Ships and Ocean Structures (CeSOS), NTNU, Trondheim, within the "Violent Water-Vessel Interactions and Related Structural Loads" project, and partially done within the framework of the "Programma di Ricerca sulla Sicurezza" funded by *Ministero Infrastrutture e Trasporti*.

References

Bagnold, R.A., 1939. Committee on wave pressures: Interim report on wave pressure research. Journal of the Institution of Civil Engineers 12, 201–226.

Faltinsen, O., Landrini, M., Greco, M., 2004. Slamming in marine application. Journal of Engineering Mathematics 48, 187–217.

Faltinsen, O.M., 1997. The effect of hydroelasticity on ship slamming. Philosophical Transactions of Royal Society London A 315, 575–591.

Greco, M., 2001. A two-dimensional study of green-water loading. Ph.D. Thesis, Department of Marine Hydrodynamics, NTNU, Trondheim, Norway. Electronic version available at URL ⟨http://www.diva-portal.org/ntnu/theses/abstract.xsql?dbid=524⟩.

Greco, M., Landrini, M., Faltinsen, O., 2003. Local hydroelastic analysis of a VLFS with shallow draft. In: 3rd International Conference on Hydroelasticity in Marine Technology. Oxford, UK, pp. 201–214.

Greco, M., Landrini, M., Faltinsen, O.M., 2004. Impact flows and loads on ship-deck structures. Journal of Fluids and Structures 19 (3), 251–275.

Greco, M., Colicchio, G., Faltinsen, O., 2006. Local and global hydroelastic analysis of a VLFS. In: 4th International Conference on Hydroelasticity in Marine Technology, Wuxi, China, pp. 225–234.

Greco, M., Colicchio, G., Faltinsen, O., 2008. Bottom slamming for a Very Large Floating Structure: Coupled global and slamming analyses. Journal of Fluids and Structures, this issue, doi:10.1016/j.jfluidstructs.2008.09.003.

Johansson, M., 1989. Barrier-type breakwaters: transmission, reflection and forces. Ph.D. Thesis, Chalmers University of Technology, Göteborg, Sweden.

Ogilvie, T.F., 1967. Nonlinear high-Froude-number free surface problems. Journal of Engineering Mathematics 1 (3), 215–235.

Ohmatsu, S., 2005. Overview: research on wave loading and responses of VLFS. Marine Structures 18, 149–168.

Ohta, M., Ohmatsu, S., 1998. Analysis and experimental verification of elastic behavior of huge floating structure in waves. In: 14th Ocean Engineering Symposium (SNAJ), pp. 475–481.

Taghipour, R., Fu, S., Moan, T., 2006. Validated two and three dimensional linear hydroelastic analysis using ABAQUS and WAMIT. In: Proceedings of the 16th International Offshore and Polar Engineering Conference (ISOPE), San Francisco, California, USA, Paper No. 2006-JSC-478.

Takagi, K., 1997. A theoretical approach to the slamming impact pressure acting on the VLFS. International Journal of Offshore and Polar Engineering 12, 9–15.

Wagner, H., 1932. Uber stoss- und gleitvorgange an der oberflache von flussigkeiten. Zeitschrift fuer Angewandte Mathematik und Mechanik 12 (4), 192–235.

Watanabe, Y., 2002. Private communication. National Maritime Research Institute. Tokyo, Japan.

Yago, K., Endo, H., 1996. Model experiment and numerical calculation of the hydroelastic behaviour of a matlike VLFS. In: International Workshop on Very Large Floating Structures (VLFS'96), Hayama, Japan, pp. 209–216.

Yoshimoto, H., Ohmatsu, K., Ohmatsuandi, S., Ikebuchi, T., 1997. Slamming load on a very large floating structure with shallow draft. Journal of Marine Science and Technology 2, 163–172.